Synthetic Molecules for Disruption of the MYC Protein-Protein Interface

*Nicholas T Jacob, Pedro O Miranda†, Ryan J Shirey, Ritika Gautam, Bin Zhou, M Elena de Orbe Izquierdo, Mark S Hixon∫, Jonathan R Hart, Lynn Ueno, Peter K Vogt, Kim D Janda**

Department of Chemistry, BCC-582, 10550 N Torrey Pines Road, The Scripps Research Institute, La Jolla, CA 92037

ABSTRACT. MYC is a key transcriptional regulator involved in cellular proliferation and has established roles in transcriptional elongation and initiation, microRNA regulation, apoptosis, and pluripotency. Despite this prevalence, functional chemical probes of MYC function at the protein level have been limited. Previously, we discovered **5a**, that binds to MYC with potency and specificity, downregulates the transcriptional activities of MYC and shows efficacy *in vivo*. However, this scaffold posed intrinsic pharmacokinetic liabilities, namely, poor solubility that precluded biophysical interrogation. Here, we developed a screening platform based on field-effect transistor analysis (Bio-FET), surface plasmon resonance (SPR), and a microtumor formation assay to analyze a series of new compounds aimed at improving these properties. This blind SAR campaign has produced a new lead compound of significantly increased *in vivo* stability and solubility for a 40-fold increase in exposure. This probe represents a significant advancement that will not only enable biophysical characterization of this interaction and further SAR, but also contribute to advances in understanding of MYC biology.

INTRODUCTION

The v-myc myeleocytomatosis viral oncogene homolog (MYC) protein is an essential regulator of cell-cycle progression occupying and apical space in the trasncriptome.[1] Importantly, MYC has been directly implicated in most human cancers and its role recognized as a hallmark of cancer initiation and maintenance.[2-6] In general, MYC expression has a strong correlation to dramatic effects on cellular proliferation and function, but the molecular determinants responsible for these effects remain controversial.[7] Part of the difficulty in studying MYC is its frenetic mode of action: although having an ephemeral existence, it is able to seemingly affect transcription in both a local and global manner. Moreover, MYC exists as an intrinsically disordered protein (IDP), taking on structure only in the presence of other basic helix-loop-helix leucine zipper (bHLH-LZ) transcription factors of the MAX network.[8,9] This lack of structure and instability greatly impairs the ability to structurally or biophysically characterize MYC interactions. In all, these attributes have worked to make MYC an attractive, but elusive target in drug discovery.

Previously, we described an inhibitory scaffold of the MYC-MAX-DNA complex, KJ-Pyr-9, **5a**.[10] This compound exhibited potent inhibition of the transforming capabilities of an oncogenic ATG-MYC virus in chicken embryo fibroblasts (CEF); importantly, it also demonstrated a higher specificity of inhibition for MYC than other oncogenes. However, the scaffold presents intrinsic liabilities: namely, a very modest solubility (~8μM), compounding the difficulty in characterizing this interaction, as well as several undesirable moieties, namely the nitro group. To overcome these obstacles, we developed a multifaceted screening platform combining *in vitro* biophysical characterization with *in vivo* methods.

RESULTS AND DISCUSSION

With no structural characterization of the interaction between **5a** and MYC, a blind SAR campaign was undertaken primarily directed at accessing a more soluble scaffold to enable formal characterization. A series of compounds with bioisosteric replacements of the undesirable moieties and aimed at increased solubility were produced via the Kröhnke pyridine synthesis. Thus, a family of α,β-unsaturated ketones **2** were synthesized using two pathways (Scheme 1): (a) Reaction of a methyl ketone bearing variety of different five-membered heterocycles such as thiazole, imidazole and triazole (b) an oxazole reaction with the corresponding acylchloride, which allowed for introduction of the oxazole moiety. A second reaction between **2** and pyridinium salts **1** (obtained from the corresponding phenacyl bromide derivative) using ammonium acetate at 100 ºC gave the corresponding 2,4,6-trisubstituted pyridines **3**. Compounds **5i-k** were obtained at this point, while all others contained a *p*-methylestergroup in the R^3 position. The methylester group of **3** was hydrolyzed to obtain carboxylic acid **4**. The carboxylic acid was reacted with oxalyl chloride and *N,N*-dimethylformamide in order to obtain the corresponding acyl chlorides, which were then reacted with different nucleophiles to form compounds **5**. In order to access truncated pyridine scaffolds, such as **7a** and **7b**, a palladium-catalyzed Suzuki cross-coupling strategy was used as shown in Scheme 2. After the preparation of these compounds, the next step was to examine their activity relative to **5a**.

Scheme 1. Synthesis of pyridine scaffolds **5a-5o**.

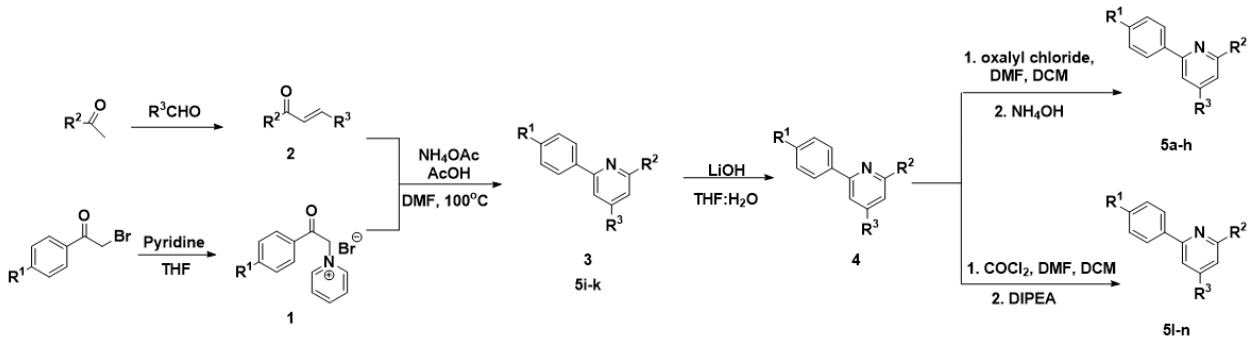

5a: R^1= NO_2; R^2= 2-furanyl; R^3 = *p*-C_6H_4-$CONH_2$
5b: R^1= CN; R^2= 2-furanyl; R^3 = *p*-C_6H_4-$CONH_2$
5c: R^1= CN; R^2= 2-thiazolyl; R^3 = *p*-C_6H_4-$CONH_2$
5d: R^1= CN; R^2= 2-oxazolyl; R^3 = *p*-C_6H_4-$CONH_2$
5e: R^1= CN; R^2= N-methyl-2-imidazolyl; R^3 = *p*-C_6H_4-$CONH_2$
5f: R^1= CN; R^2= 1-methy-1*H*-1,2,3-triazol-5-yl; R^3 = *p*-C_6H_4-$CONH_2$
5g: R^1= 2-thiazolyl; R^2= 2-furanyl; R^3 = *p*-C_6H_4-$CONH_2$
5h: R^1= 5-oxazolyl; R^2= 2-furanyl; R^3 = *p*-C_6H_4-$CONH_2$

5i: R^1= CN; R^2= 2-furanyl; R^3 = C_6H_5
5j: R^1= 2-thiazolyl; R^2= 2-furanyl; R^3 = 2-thiazolyl
5k: R^1= CN; R^2= 2-furanyl; R^3 = *p*-C_6H_4-CN_4H
5l: R^1= CN; R^2= 2-furanyl; R^3 = *p*-C_6H_4-$CONHMe$
5m: R^1= CN; R^2= 2-furanyl; R^3 = *p*-C_6H_4-$CONHSO_2Me$
5n: R^1= CN; R^2= 2-furanyl; R^3 = *p*-C_6H_4-$CONHNH_2$
5o: R^1= CN; R^2= *m*-C_6H_4F; R^3 = *p*-C_6H_4-$CONH_2$

Scheme 2. Synthesis of pyridine scaffolds **7a** and **7b**.

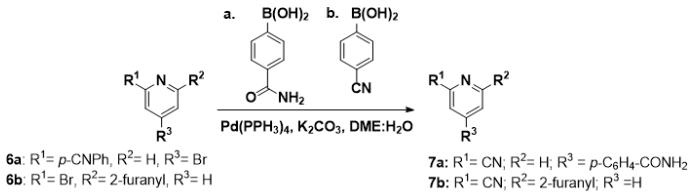

Initially, compound solubilities were measured by dynamic light scattering (Table 1). In order to screen new compounds for MYC binding, a field-effect transistor (Bio-FET) was used. Bio-FET offers several advantages for characterizing this interaction[11,12]: 1. A much lower limit of detection as compared with SPR or isothermal calorimetry. 2. Detection being conducted on a graphene surface, which reduces the interaction of the disordered protein with the chip surface. 3. Site-specific functionalization, which reduces the amount of noise caused from aggregates on the chip surface. The basic-helix-loop-helix (bHLH) motif of MYC has been established a solvent-accessible region critical for MYC function.[10,13] A His-tagged bHLH construct was immobilized on the chip (see Materials and Methods) and compounds screened for interaction. We were able to observe saturation of surface-bound MYC across chips at 10 µM **5a** in 3% DMSO in MES buffer to give a maximal response signal. This was used as the control on each chip screened and gave a benchmark in terms of both solubility and affinity for the protein (Figure 1a, Table 1). Compounds were screened by measuring the chip response at 10 µM and normalized to the response found for **5a** in that run. All compounds were also screened against a monomeric form of MAX (mMAX), as well as MYC-MAX and MAX-MAX dimers (see Supplemental Material). The lack of observed binding to mMAX, MAX-MAX and the unbound control surface, as well as the general ability to regenerate the chip surface, indicates that there is a specificity in the observed binding interactions.

The affinity of the MYC-MAX interaction is relatively weak (K_d = 176 nM[14]), making measurement of the perturbation in this interaction difficult. However, positive results have been obtained measuring the binding affinity for DNA using a stabilized MYC-MAX complex.[10] Using surface plasmon

resonance (SPR), we established a characteristic binding response of stabilized MYC-MAX dimers to immobilized E-BOX oligonucleotides on the chip surface. Heterodimers were stabilized through disulfide formation through a C-terminal cystine residue introduced to the MYC bHLH and MAX constructs. This stabilization was found necessary to prevent aggregation of MYC monomer on the chip surface during runs. Incubation of dimer with treatment compound prior to flowing over the chip surface showed a perturbation in the sensogram when compared to the vehicle control. Compounds were incubated with dimer at 10 μM and their ability to prevent interaction with DNA measured (Figure 1b). Importantly, compounds observed to have no interaction with MYC were also found to have no effect in preventing dimer binding to DNA, and no interaction was observed between the DNA and compounds alone.

Table 1: Activity summary.

ID	MW	Solubility (µM)[a]	FET R_{eq} (%)[b]	CEF IC_{50} (µM)[c]
5a	385.4	8	100	1
5b	365.4	10	106	3
5c	382.4	64	79	30
5d	299.3	250	0	>100
5e	379.4	8	41	40
5f	380.4	32	55	40
5g	423.5	125	97	5
5h	407.4	15	154	2.5
5i	366.4	2	72	5
5j	387.5	< 1	188	>100
5k	390.4	18	92	2
5l	379.4	25	3.2	NT
5m	443.5	32	76	10
5n	380.4	500	0	>100
5o	393.4	2	0	>100
7a	322.4	32	0	10[d]
7b	246.3	10	0	NT
10a	366.4	8	66	7
10b	381.4	< 1	0	>100
10c	393.4	25	0	>100

a – Measured by DLS in MES (pH 6.0) with < 0.1 % DMSO. b – Relative to 5a R_{eq}. c – Measured in CEF transfected with ATG-MYC. d – inhibited all cell growth. NT – not tested.

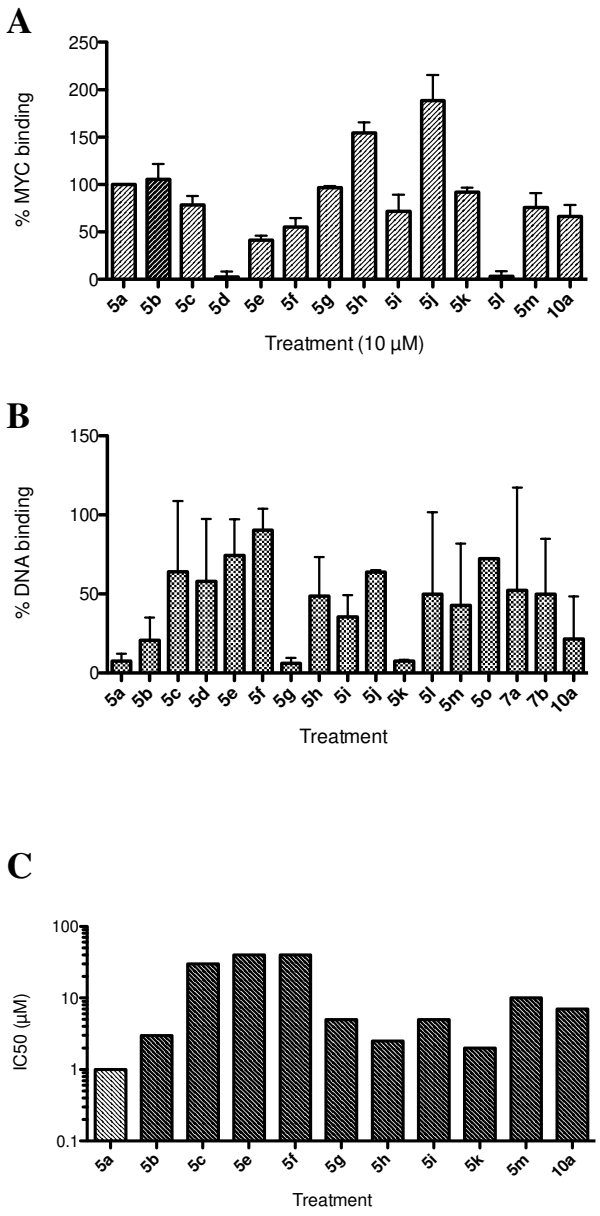

Figure 1: Activity screening of test compounds. a) Relative binding to MYC compared with **5a**. b) Inhibition of MYC-MAX binding to DNA measured by SPR. c) IC_{50} of optimized compounds in CEF assay. Error bars are SEM, n = 3.

The ultimate assessment of anti-MYC activity was done through a well-established focus assay examining the ability of an ATG-MYC expressing vector to establish microtumors in CEF.[15] Compelling compounds from binding studies were examined for inhibition of microtumor formation in

this assay (Figure 1c). Several derivatives were found to inhibit microtumor formation with similar efficacy to **5a** (Table 1). Overall, the CEF and FET data correlated well (Supplemental Figure 1), apart from **5j**, which was of much poorer solubility than **5a**. This was opposed to the SPR data, which did not correlate well with either the FET or CEF data. We reason that this discrepancy is due to the covalent linkage of the MYC-MAX dimers, which alters the affinity necessary to perturb the complex greatly. Additionally, the MYC-MAX-DNA complex is far more stable than the heterodimer itself (Fieber, JMB, 2001), and thus shifts the equilibrium of MYC-MAX heterodimerization. We also note that while the FET and CEF data correlate very well, there is a discrepancy between the affinity for MYC and the potency in cells. This is a common pharmacodynamic phenomenon when targeting protein-protein interactions. *MYC* is pleiotropic, the MYC-MAX complex coordinates and controls the expression of thousands of other genes, and thus the precise molecular determinants responsible for any observed phenotype related to a change in MYC concentration are unknown. The intervening factors will be illuminated by further studies of MYC biology with an effective inhibitor.

The results of these experiments provide the beginnings of a structure-activity map for MYC inhibition. In general, the whole framework of **5a** appears necessary as compounds **7a** and **7b** lost all activity when entire substituents of the central pyridine were eliminated. This may indicate the "Y-shape" of the scaffold is a necessary pharmacophore. Critically, the most prominent liability, the p-nitro moiety in R^1, was found dispensable, able to be effectively replaced with a cyano (**5b**) or thiazole heterocycle (**5g**). This also assuaged concerns that inhibition proceeds through a covalent mechanism.

By contrast, it was found there was little plasticity in the chemical space of the furan substituent at the R^2 position. Elimination of the furan ablated activity (**7a**) and replacement with another heterocycle resulted in a loss or significant attenuation of activity (**5d**, **5f**, and **5o**). In general, there are concerns that furan functionality is prone to oxidation and the formation of reactive metabolites,[16] however, it was not known the degree to which this moiety presented a pharmacokinetic liability in these particular scaffolds. We reasoned that the π-conjugation throughout the scaffold would impart increased stability to the furan from oxidation. To test this, we examined the stability of several compounds incubated with

rat liver microsomes (Figure 2). We found that while the nitro group of **5a** was readily eliminated, the furan was exceedingly recalcitrant to oxidation in these conditions. Importantly, the mass of oxidized furan ion was not detected.

Ablation of the p-benzylamide lost all activity (**7b**), but complete replacement of the p-benzylamide in **5j** was the only compound found to have significantly greater binding to MYC than **5a**, indicating a pliability. However, the solubility was reduced and it was not found to have any activity in the CEF assay. We reason that the lack of aqueous solubility even at low doses completely precludes cell penetration. In a similar vein, carboxylic acids of **4** were also found inactive in both the Bio-FET and CEF assays. However, it was found there was significant plasticity in the space around the amide substituent. The use of a *N*-methylsulfonyl benzamide in **5m** had a modest improvement in solubility, but it was found less

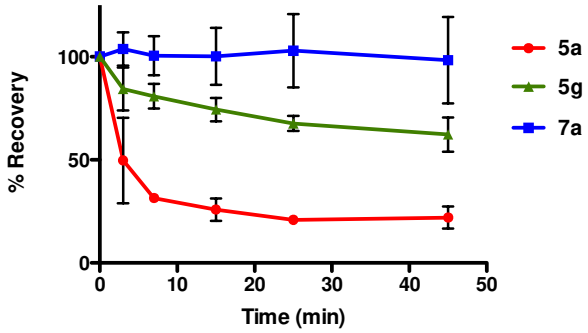

Figure 2: Oxidation susceptibility by rat liver microsomes by mass analysis. Compounds were incubated with microsomes at 37 ºC for indicated time. Recovery calculated from AUC of extracted ion.

effective in binding MYC and had a 10-fold loss of potency compared to **5a**. Similar results were obtained with **5k**, containing a tetrazole in place of the amide, indicating an advanced plasticity in this region.

Importantly, it was also found that changes to the core heterocycle were tolerated. Diversity was introduced into the core heterocycle with the formation of a pyrimidine ring in an attempt to optimize solubility. An α,β-unsaturated ketone **2i** was refluxed with furancarboximidine **8** in the presence of

excess sodium methoxide in ethanol to produce carboxylic acid **9**, which was converted to the corresponding amide via the same strategy of forming acylchloride and reacting it with NH_4OH to give pyrimidine **10** (Scheme 3). **10a** has an activity profile comparable to **5a**. Further diversification of the scaffold using a pyrimidine core presents an opportunity to produce more soluble derivatives.

Scheme 3. Pyrimidine synthesis.

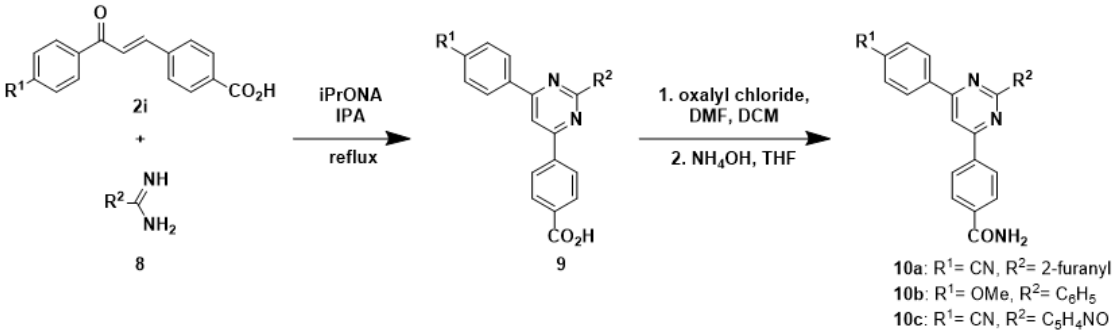

Overall, **5g** is ideal in that it is readily accessed, has greatly increased solubility, lacks the labile nitro group, and demonstrates similar binding and efficacy to **5a**. The affinity of **5g** is 12.5 ± 4.1 nM, comparable to the affinity measured for **5a** of 6.5 ± 2.6 nM (Supplementary Figure 4). A 10 mg/kg i.v. PK study was conducted in mouse to determine if these favored properties translated into improved PK. Non-compartmental analysis of the mouse PK followed by allometric scaling to the rat afforded a comparison to the rat PK study conducted previously[10] on **5a** and is shown in Table 2. This relatively simple substitution has significantly increased the mean residence time from 1 hour to 4.8 producing a 30-fold improvement in exposure (AUC) (Supplementary Figure 6). Replacement of the nitro group, along with the increased solubility, stability and concomitant increase in PK, make **5g** a significant improvement on this scaffold, with little cost to ligand efficiency (LE). The LE of **5a** and **5g** was found to be 0.40 and 0.36, respectively (Supplementary Table 1). This demonstrates that there is sufficient plasticity in the chemical space discovered through **5a** to improve the physiochemical properties without compromising efficacy.

Table 2. PK comparison of **5a** and **5g**.

	5a[a]	**5a**[b]	**5g**[c]
MW (g/mol)	385.3	385.3	423.5
Half-life (h)	1.6	1.0	4.8
AUC (ng*h/mL)	258	1,450	44,000
MRT (h)	1.7	0.94	4.3
Vss (L)	6.44	6.44	0.97
CI (mL/min/kg)	65	115	3.8

[a] – values determined in Sprague Dawley rat [b] – values are allometrically scaled from those determined in rat.[10] [c] – values determined in C57Bl6 mice.

CONCLUSION

Through analysis of a blind SAR campaign, we developed a new series of compounds that retain the efficacy of **5a**, but with improved *in vivo* stability and solubility. We hypothesize there is a goldilocks effect, whereby the hydrophobicity imparted by the conjugation of the scaffold is intrinsically necessary for binding to MYC, but this hydrophobicity negatively affects the pharmacokinetic properties of such a molecule. Thus, the slight activity compromise of **5g** for the sake of solubility may represent an optimally balanced scaffold for targeting MYC. The necessary potency of a MYC inhibitor for *in vivo* efficacy remains to be delineated. **5g** provides new opportunities assessing the balance between retaining target level potency while optimizing drug-like properties. This information will help to open access to thorough biophysical characterization of this inhibition interaction to allow for a structure-based SAR campaign to be undertaken.

EXPERIMENTAL SECTION

All solvents and chemicals were acquired from Thermo-Fisher or Millipore Sigma unless otherwise specified. Solvent was anhydrous unless otherwise specified. Purification of compounds was carried out by prep TLC on 1mm PLC silica gel 60 F_{254} plates and by flash chromatography on a Teledyne ISCO Combiflash Rf + Lumen. Compounds and intermediates were characterized by NMR on a Bruker DPX-400 or NEO-500 instrument in indicated solvent, and high-resolution mass-spectrometry on an Agilent ESI-TOF. Purity of > 95% was determined by HPLC analysis on an Agilent 1260 Infinity (see Supplement). Compounds were screened for known PAINS compounds through 2 database searches (ZINC Patterns, FAF-Drugs4).

General Procedure for compounds 5a-o. Chalcone **2** (1g, 4 mmol.), and NH_4OAc (9.2 g, 120 mmol) were dissolved in a mixture of acetic acid (20 mL) and DMF (30 mL). To it, pyridinium salt **1** (1.2 g. 4 mmol) was added and the reaction mixture was heated at 100 ºC overnight. Solvent was evaporated under vacuum and the remaining brown oil was dissolved in DCM (100 mL) and solid $NaHCO_3$ was added until the gas release ceased. The organic phase was dried over $MgSO_4$ and evaporated under reduced pressure. The product **3** is crashed out using Et_2O-MeOH as a brown solid. This material was carried on without further purification. LiOH (2.5 g, 104 mmol) was added to a solution of **3** in THF:H_2O (9:1) and stirred overnight. The reaction mixture was filtered through a pad of silica gel and evaporated to dryness to afford carboxylic acid **4**. **4** (3g, 8.2 mmol.) was dissolved in dry DCM (100 mL) and oxalyl chloride (0.7 mL, 8.2 mmol) followed by 1 drop of DMF. The reaction was stirred at room temperature overnight, then the solvent was removed in vacuo and the remaining solid was redissolved in dry DCM (100 mL). The solution was poured onto a NH_4OH solution (50 mL) and the reaction mixture was stirred for 30 min. The organic layer was separated, dried and evaporated under vacuo to afford a brown oil which was purified to obtain pyridine **5**.

5b: ^{1}HNMR (600 MHz, DMSO-d_6): δ = 8.54 (d, J = 12 Hz, 2H), 8.35 (s, 1H), 8.12 (m, 3H), 8.08 (d, J = 6 Hz, 2H), 8.04 (d, J = 12 Hz, 2H), 7.94 (s, 1H), 7.50 (brs, 1H), 7.42 (s, 1H), 6.75 (s, 1H); ^{13}CNMR (150 MHz, DMSO-d_6): δ = 167.23, 154.81, 152.78, 149.39, 148.74, 144.66, 142.48, 139.50, 134.99,

132.70, 128.25, 127.77, 127.19, 118.83, 117.28, 115.59, 112.48, 111.77, 110.14; HRMS (ESI-TOF) : *m/z* calcd for $C_{24}H_{17}N_3O_2$: 366.1237 $(M + H)^+$; found: 366.1238.

5c: ^{1}HNMR (600 MHz, DMSO-d_6): δ = 8.54 (m, 3H), 8.47 (d, *J* = 12 Hz, 1H), 8.16 (brs, 1H), 8.15 (d, *J* = 6 Hz, 2H), 8.10-8.07 (m, 5H), 8.00 (d, *J* = 6 Hz, 1H), 7.51 (brs, 1H); ^{13}CNMR (150 MHz, DMSO-d_6): δ = 167.98, 167.20, 155.01, 151.43, 149.35, 144.47, 141.78, 139.12, 135.21, 132.87, 128.35, 127.75, 127.27, 123.37, 119.94, 118.76, 116.21, 112.08; HRMS (ESI-TOF) : *m/z* calcd for $C_{22}H_{14}N_4OS$: 383.0961 $(M + H)^+$; found: 383.0960.

5d: ^{1}HNMR (600 MHz, DMSO-d_6): δ = 8.58 (s, 1H), 8.56 (d, *J* = 6 Hz, 2H), 8.44 (s, 1H), 8.41 (s, 1H), 8.16 (brs,1H), 8.15 (d, *J* = 6 Hz, 2H), 8.09 (d, *J* = 6 Hz, 2H), 8.06 (d, *J* = 6 Hz, 2H), 7.56 (s, 1H), 7.51 (s, 1H); ^{13}CNMR (150 MHz, DMSO-d_6): δ = 167.19, 159.87, 155.32, 149.11, 146.41, 142.04, 141.50, 138.94, 135.23, 132.80, 128.99, 128.35, 127.90, 127.28, 120.01, 119.00, 118.75, 112.03; HRMS (ESI-TOF) : *m/z* calcd for $C_{22}H_{14}N_4O_2$: 367.1189 $(M + H)^+$; found: 367.1183.

5e: ^{1}HNMR (600 MHz, DMSO-d_6): δ = 8.51 (d, *J* = 6 Hz, 2H), 8.45 (d, *J* = 6Hz, 1H), 8.41 (d, *J* = 1.5 Hz, 1H), 8.15 (brs, 1H), 8.09 (d, *J* = 3Hz, 4H), 8.03 (d, *J* = 6 Hz, 2H),7.96 (d, *J* = 12 Hz, 2H), 7.50 (brs, 1H), 7.42 (s, 1H), 7.11 (d, *J* = 1 Hz, 1H), 4.23 (s, 3H); ^{13}CNMR (150 MHz, DMSO-d_6): δ = 167.25, 154.25, 151.18, 148.53, 143.60, 142.73, 139.54, 135.02, 132.83, 132.38, 128.36, 128.00, 127.09, 125.79, 119.09, 118.81 117.64, 111.75, 36.47; HRMS (ESI-TOF) : *m/z* calcd for $C_{23}H_{17}N_5O$: 380.1506 $(M + H)^+$; found: 380.1504.

5f: ^{1}HNMR (600 MHz, DMSO-d_6): δ = 8.60 (s, 1H), 8.53 (d, *J* = 6 Hz, 2H), 8.50 (s, 1H), 8.36 (s, 1H), 8.20 (d, *J* = 6 Hz, 2H), 8.16 (brs, 1H), 8.09 (d, J = 12 Hz, 2H), 8.05 (d, J = 12 Hz, 2H), 7.53 (brs, 1H), 4.50 (s, 3H); ^{13}CNMR (150 MHz, DMSO-d_6): δ = 167.18, 155.05, 149.18, 147.61, 142.36, 139.00, 135.62, 135.17, 134.48, 132.85, 128.20, 127.91, 127.39, 120.20, 119.50, 118.75, 118.45, 112.0, 37.96; HRMS (ESI-TOF) : *m/z* calcd for $C_{22}H_{16}N_6O$: 381.1458 $(M + H)^+$; found: 381.1457.

5g: ^{1}HNMR (600 MHz, DMSO-d_6): δ = 8.46 (d, *J* = 12 Hz, 2H), 8.28 (s, 1H), 8.16 (brs, 1H), 8.12 (m, 3H), 8.08 (d, *J* = 12 Hz, 2H), 8.00 (d, J = 3 Hz, 1H), 7.94 (s, 1H), 7.86 (s, d, J = 3 Hz, 1H), 7.51

(brs, 1H), 7.40 (s, 1H), 6.75 (s, 1H); ^{13}CNMR (150 MHz, DMSO-d_6): δ = 167.29, 166.58, 155.80, 153.00, 149.26, 148.55, 144.50, 144.08, 139.78, 139.67, 134.90, 133.78, 128.77, 127.77, 127.13, 126.48, 120.88, 116.62, 114.92, 112.43, 109.89; HRMS (ESI-TOF) : *m/z* calcd for $C_{25}H_{17}N_3O_2S$: 424.1114 $(M + H)^+$; found: 424.1116.

5h: ^{1}HNMR (600 MHz, DMSO-d_6): δ = 8.52 (s, 1H), 8.45 (d, *J* = 12 Hz, 2H), 8.27 (s, 1H), 8.15 (brs, 1H), 8.12 (m, 3H), 8.04 (s, 1H), 7.93 (m, 3H), 7.94 (s, 1H), 7.84 (s, 1H), 7.50 (brs, 1H), 7.39 (s, 1H), 6.74 (s, 1H); ^{13}CNMR (150 MHz, DMSO-d_6): δ = 167.28, 155.89, 153.03, 152.14, 150.21, 149.21, 148.51, 144.48, 139.81, 138.18, 134.88, 128.25, 128.17, 127.68, 127.13, 124.35, 122.81, 116.45, 114.76, 112.42, 109.84; HRMS (ESI-TOF) : *m/z* calcd for $C_{25}H_{17}N_3O_3$: 408.1343 $(M + H)^+$; found: 408.1350.

5i: ^{1}HNMR (600 MHz, $CDCl_3$): δ = 8.28 (d, *J* = 12 Hz, 2H), 7.96 (s, 1H), 7.85 (s, 1H), 7.82 (d, *J* = 12 Hz, 2H), 7.78 (d, J = 6 Hz, 2H), 7.61 (s, 1H), 7.58-7.52 (m, 3H), 7.27 (s, 1H), 6.62 (s, 1H); ^{13}CNMR (150 MHz, $CDCl_3$): δ = 154.94, 153.20, 150.02, 149.62, 143.12, 142.98, 137.76, 132.07, 128.92, 128.75, 127.18, 126.63, 118.43, 116.77, 115.67, 112.07, 111.76, 109.01; HRMS (ESI-TOF) : *m/z* calcd for $C_{22}H_{14}N_2O$: 323.1179 $(M + H)^+$; found: 323.1182.

5j: ^{1}HNMR (600 MHz, DMSO-d_6): δ = 8.37 (d, *J* = 12 Hz, 2H), 8.31 (s, 1H), 8.15 (s, 1H), 8.12 (s, 1H), 8.11 (d, *J* = 12 Hz, 2H), 8.05 (d, J = 6 Hz, 1H), 8.00 (d, *J* = 6Hz, 1H), 7.94 (s, 1H), 7.86 (s, 1H), 7.37 (s, 1H), 6.74 (s, 1H); ^{13}CNMR (150 MHz, DMSO-d_6): δ = 166.48, 164.37, 156.18, 152.55, 149.47, 144.83, 144.51, 144.09, 141.89, 139.04, 133.99, 127.67, 126.58, 123.05, 120.95, 114.96, 113.28, 112.53, 110.20; HRMS (ESI-TOF) : *m/z* calcd for $C_{21}H_{13}N_3OS_2$: 388.0573 $(M + H)^+$; found: 388.0574.

5k: ^{1}HNMR (600 MHz, DMSO-d_6): δ = 8.54 (d, *J* = 12 Hz, 2H), 8.34 (s, 1H), 8.18 (d, *J* = 12Hz, 2H), 8.11 (s, 1H), 8.07 (d, *J* = 12 Hz, 2H), 8.03 (d, *J* = 12 Hz, 3H), 7.94 (s, 1H), 7.41 (s, 1H), 6.74 (s, 1H); ^{13}CNMR (150 MHz, DMSO-d_6): δ = 160.11, 154.69, 152.94, 149.45, 149.31, 144.53, 142.68, 135.00, 134.00, 132.68, 127.74, 127.26, 126.28, 118.86, 116.79, 115.05, 112.42, 111.64, 109.90; HRMS (ESI-TOF) : *m/z* calcd for $C_{23}H_{14}N_6O$: 391.1302 $(M + H)^+$; found: 391.1315.

Scheme for synthesis of compounds 5m-5o

Carboxylic acid **4a** (1g, 2.7 mmol.) was dissolved in dry DCM (100 mL) and oxalyl chloride (0.5 mL, 5 mmol) followed by DMF (1 drop) were added. The reaction was stirred at room temperature overnight. Then, the solvent was removed in vacuo and the remaining solid was redissolved in dry DCM (100 mL). The solution was poured onto a solution of (a) methylamine and DIPEA (1:1) (25 mL); (b) methanesulfonamide (300 mg, 3.15 mmol) and DIPEA (10 mL) or (c) hydrazine and DIPEA (1:1) (25 mL) and the reaction mixture was stirred for 30 min. Then, the organic layer was washed with water, separated, dried and evaporated under vacuo to afford **5l**, **5m** and **5n** respectively. The products were purified by prep TLC using DCM/MeOH (85:15) as eluent.

5l: ^{1}HNMR (600 MHz, DMSO-d6): δ = 8.63 (m, 2H), 8.53 (d, *J* = 12 Hz, 2H), 8.35 (s, 1H), 8.14 (d, *J* = 12 Hz, 2H), 8.11 (s, 1H), 8.04 (m, 3H), 7.94 (s, 1H), 7.42 (s, 1H), 6.74 (s, 1H), 2.84 (s, 3H); ^{13}CNMR (150 MHz, DMSO-d6): δ = 165.92, 154.82, 152.78, 149.39, 148.70, 144.66, 142.48, 139.29, 135.19, 132.70, 127.83, 127.77, 127.24, 118.83, 117.25, 115.55, 112.48, 111.77, 110.13; HRMS (ESI-TOF) : *m/z* calcd for $C_{24}H_{17}N_3O_2$: 380.1393 $(M + H)^+$; found: 380.1394.

5m: ^{1}HNMR (600 MHz, DMSO-d6): δ = 8.54 (d, *J* = 6 Hz, 2H), 8.32 (s, 1H), 8.12 (d, *J* = 6 Hz, 2H), 8.08 (s, 1H), 8.01 (m, 4H), 7.94 (brs, 1H), 7.93 (s, 1H), 7.40 (s, 1H), 6.74 (m, 1H), 2.89 (s, 3H); ^{13}CNMR (150 MHz, DMSO-d6): δ = 169.75, 154.73, 152.86, 149.32, 144.57, 142.58, 140.75, 137.93, 132.68, 129.74, 129.00, 127.76, 126.34, 118.85, 117.10, 115.40, 112.43, 111.68, 109.98, 43.13 ; HRMS (ESI-TOF) : *m/z* calcd for $C_{24}H_{17}N_3O_4S$: 444.1012 $(M + H)^+$; found: 444.1017.

5n: ^{1}HNMR (600 MHz, DMSO-d6): δ = 9.96 (s, 1H), 8.54 (d, *J* = 12 Hz, 2H), 8.35 (s, 1H), 8.14 (d, *J* = 6 Hz, 2H), 8.11 (s, 1H), 8.03 (d, *J* = 12 Hz, 3H), 7.94 (s, 1H), 7.41 (s, 1H), 6.75 (s, 1H), 4.57 (s, 2H); ^{13}CNMR (150 MHz, DMSO-d6): δ = 165.11, 154.81, 152.77, 149.39, 148.69, 144.66, 142.48, 139.34, 134.01, 132.70, 127.76, 127.27, 118.82, 117.24, 115.55, 112.47, 111.77, 110.13 ; HRMS (ESI-TOF) : *m/z* calcd for $C_{23}H_{16}N_4O_2$: 381.1346 $(M + H)^+$; found: 381.1358.

Synthesis of 7a

To a solution of 4-bromo-2-(4-cyanophenyl)pyridine (200 mg, 0.77 mmol.) in dry DME (3 mL) was added 4-aminocarbonyl phenyl boronic acid (152 mg, 0.80 mmol.) and water (1 mL). Then, K_2CO_3 (320

mg, 2.3 mmol.) and $Pd(PPh_3)_4$ (36 mg, 0.03 mmol.) were added and the reaction heated at 85 ºC overnight. The reaction mixture was evaporated, adsorbed over silica gel and purified by column chromatography using EtOAc as eluent to afford **7a** as a white solid (160 mg). ^{1}HNMR (600 MHz, DMSO-d_6): δ = 8.82 (d, *J* = 6 Hz, 1H), 8.45 (m, 3H), 8.13 (brs, 1H), 8.06 (m, 4H), 7.84 (d, *J* = 6 Hz, 1H), 7.49 (brs, 1H); ^{13}CNMR (150 MHz, DMSO-d_6): δ = 167.25, 154.98, 150.54, 147.61, 142.84, 139.54, 134.89, 132.69, 128.25, 127.66, 127.09, 121.28, 118.83, 111.60; HRMS (ESI-TOF) : *m/z* calcd for $C_{19}H_{13}N_3O$: 300.1131 $(M + H)^+$; found: 300.1132.

Synthesis of 7b

To a solution of 2-bromo-6-(furan-2-yl) pyridine (280 mg, 1.25 mmol.) in dry DME (3 mL) was added 4-cyanophenyl boronic acid (220 mg, 1.3 mmol.) and water (1 mL). Then, K_2CO_3 (520 mg, 3.75 mmol.) and $Pd(PPh_3)_4$ (60 mg, 0.05 mmol.) were added and the reaction heated at 85 ºC overnight. The reaction mixture was evaporated, adsorbed over silica gel and purified by column chromatography using Hex/EtOAc (8:2) as eluent to afford **7b** as a white solid (180 mg). ^{1}HNMR (600 MHz, $CDCl_3$): δ = 8.23 (d, *J* = 6 Hz, 2H), 7.86 (t, *J* = 6 Hz, 1H), 7.80 (m, 1H), 7.73 (d, J = 6 Hz, 1H), 7.66 (d, J = 6 Hz, 1H), 7.59 (s, 1H), 7.22 (s, 1H), 6.60 (m, 1H); ^{13}CNMR (150 MHz, $CDCl_3$): δ = 154.24, 153.10, 149.15, 143.11, 142.84, 137.26, 132.05, 127.04, 118.42, 117.52, 111.69, 108.78; HRMS (ESI-TOF) : *m/z* calcd for $C_{16}H_{10}N_2O$: 247.0866 $(M + H)^+$; found: 247.0866.

General Procedure for compounds 10a-c. To a solution of furancarboximidine **8** (250 mg, 1.72 mmol) in IPA (20 mL) was added Na (45 mg, 2 mmol) and the reaction was refluxed for 2 hrs. Afterwards, **2** (500 mg, 1.72 mmol) was added and the mixture was refluxed overnight. Then, it was evaporated to dryness under vacuum, dissolved in DCM:MeOH (8:2) and filtered through a pad of silica gel. The filtrate was evaporated to dryness to give a red oil. Carboxylic acid **9** was precipitated using EtOAc:Hex (1:1) as a yellow solid (55%). This material was carried on without further purification. **9** (200 mg, 0.55 mmol) was dissolved in DCM (20 mL) and oxalyl chloride (0.2 mL, 36 mmol) followed by 1 drop of DMF. The reaction was stirred at room temperature overnight. Solvent was removed in vacuo and the remaining solid was redissolved in DCM (50 mL). The solution was poured onto a

NH_4OH solution (50 mL) and the reaction mixture was stirred for 30 min. The organic layer was separated, dried and evaporated under vacuo to afford a brown oil which was purified to obtain pyrimidine **10**.

10a: ^{1}HNMR (600 MHz, DMSO-d6): δ = 8.66 (s, 1H), 8.65 (d, *J* = 2 Hz, 2H), 8.55 (d, *J* = 12 Hz, 2H), 8.18 (s, 1H), 8.10 (m, 4H), 8.03 (s, 1H), 7.60 (s, 1H), 7.55 (s, 1H), 6.79 (s, 1H); ^{13}CNMR (150 MHz, DMSO-d6): δ = 167.24, 163.91, 162.60, 157.33, 151.72, 146.12, 140.41, 138.39, 136.65, 132.89, 128.20, 128.04, 127.35, 118.55, 114.35, 113.49, 112.61, 111.30; HRMS (ESI-TOF) : *m/z* calcd for $C_{22}H_{14}N_4O_2$: 367.1189 $(M + H)^+$; found: 367.1202.

10b: ^{1}HNMR (400 MHz, DMSO-d6): δ = 8.35 (d, 2H), 8.22 (m, 1H), 8.10 (d, 2H), 7.82 (bs, 2H), 7.90 (m, 4H), 7.80 (d, 2H), 7.50 (m, 3H); HRMS (ESI-TOF) : *m/z* calcd for $C_{22}H_{16}N_4O$: 377.1402 $(M + H)^+$; found: 377.1482.

10c: ^{1}HNMR (400 MHz, DMSO-d6): δ = 8.66 (s, 1H), 8.65 (d, *J* = 2 Hz, 2H), 8.55 (d, *J* = 12 Hz, 2H), 8.18 (s, 1H), 8.10 (m, 4H), 8.03 (s, 1H), 7.60 (s, 1H), 7.55 (s, 1H), 6.79 (s, 1H); HRMS (ESI-TOF) : *m/z* calcd for $C_{22}H_{16}N_4O$: 382.1555 $(M + H)^+$; found: 382.1482.

ASSOCIATED CONTENT

Supporting Information.

Supplementary figures, biological protocols, sensogram data, compound characterizations, and expanded synthetic procedures (PDF)

Molecular formula strings (CSV)

AUTHOR INFORMATION

Corresponding Author

*E-mail: kdjanda@scripps.edu

Present Addresses

† Instituto de Productos Naturales y Agrobiología, CSIC, Avda. Franscisco Sánchez 3, 38206 La Laguna, Tenerife, Spain. ∫ Mark S. Hixon Consulting LLC, 11273 Spitfire Road, San Diego, CA 92126.

Author Contributions

The manuscript was written through contributions of all authors. All authors have given approval to the final version of the manuscript.

Notes

This is manuscript number 29684 from the Scripps Research Institute.

ACKNOWLEDGMENT

This work was supported by the Skaggs Institute for Chemical Biology and the National Institutes of Health (CTSA TL1TR001113 to N.T.J), and the Seventh Framework Program of the European Union (REA Grant Agreement No. 623155 to P.O.M.).

ABBREVIATIONS

FET, field-effect transistor; SPR, surface plasmon resonance; bHLH, basic-helix-loop-helix; DLS, dynamic light scattering; TLC, thin layer chromatography.

REFERENCES

(1) Adhikary, S.; Eilers, M. Transcriptional Regulation and Transformation by Myc Proteins. Nat. Rev. Mol. Cell Biol. 2005, 6 (8), 635–645.

(2) Eilers, M.; Eisenman, R. N. Myc's Broad Reach. Genes & Development 2008, 22 (20), 2755–2766.

(3) Varlakhanova, N. V.; Knoepfler, P. S. Acting Locally and Globally: Myc's Ever-Expanding Roles on Chromatin. Cancer Res. 2009, 69 (19), 7487–7490.

(4) Gabay, M.; Li, Y.; Felsher, D. W. MYC Activation Is a Hallmark of Cancer Initiation and Maintenance. Cold Spring Harb Perspect Med 2014, 4 (6), a014241–a014241.

(5) Dang, C. V. MYC on the Path to Cancer. Cell 2012, 149 (1), 22–35.

(6) Ruggero, D. The Role of Myc-Induced Protein Synthesis in Cancer. Cancer Res. 2009, 69 (23), 8839–8843.

(7) Kress, T. R.; Sabò, A.; Amati, B. MYC: Connecting Selective Transcriptional Control to Global RNA Production. Nat Rev Cancer 2015, 15 (10), 593–607.

(8) Conacci-Sorrell, M.; McFerrin, L.; Eisenman, R. N. An Overview of MYC and Its Interactome. Cold Spring Harb Perspect Med 2014, 4 (1), a014357–a014357.

(9) McKeown, M. R.; Bradner, J. E. Therapeutic Strategies to Inhibit MYC. Cold Spring Harb Perspect Med 2014, 4 (10), a014266.

(10) Hart, J. R.; Garner, A. L.; Yu, J.; Ito, Y.; Sun, M.; Ueno, L.; Rhee, J. K.; Baksh, M. M.; Stefan, E.; Hartl, M.; Bister, K.; Vogt, P. K.; Janda, K. D. Inhibitor of MYC Identified in a Krohnke Pyridine Library. Proceedings of the National Academy of Sciences 2014, 111 (34), 12556–12561.

(11) Lerner, M. B.; Pan, D.; Gao, Y.; Locascio, L. E.; Lee, K.-Y.; Nokes, J.; Afsahi, S.; Lerner, J. D.; Walker, A.; Collins, P. G.; Oegema, K.; Barron, F.; Goldsmith, B. R. Large Scale Commercial Fabrication of High Quality Graphene-Based Assays for Biomolecule Detection. Sensors and Actuators B: Chemical 2017, 239, 1261–1267.

(12) Wang, L.; Estrela, P.; Huq, E.; Li, P.; Thomas, S.; Ferrigno, P. K.; Paul, D.; Adkin, P.; Migliorato, P. Fabrication of BioFET Linear Array for Detection of Protein Interactions. Microelectronic Engineering 2010, 87 (5-8), 753–755.

(13) Kerkhoff, E.; Bister, K.; Klempnauer, K. H. Sequence-Specific DNA Binding by Myc Proteins. Proc. Natl. Acad. Sci. U.S.A. 1991, 88 (10), 4323–4327.

(14) Hu, J.; Banerjee, A.; Goss, D. J. Assembly of B/HLH/Z Proteins C-Myc, Max, and Mad1 with Cognate DNA: Importance of Protein-Protein and Protein-DNA Interactions. Biochemistry 2005, 44 (35), 11855–11863.

(15) Bos, T. J.; Monteclaro, F. S.; Mitsunobu, F.; Ball, A. R.; Chang, C. H.; Nishimura, T.; Vogt, P. K. Efficient Transformation of Chicken Embryo Fibroblasts by C-Jun Requires Structural Modification in Coding and Noncoding Sequences. Genes & Development 1990, 4 (10), 1677–1687.

(16) Peterson, L. A. Reactive Metabolites in the Biotransformation of Molecules Containing a Furan Ring. Chemical research in toxicology 2013, 26 (1), 6–25.

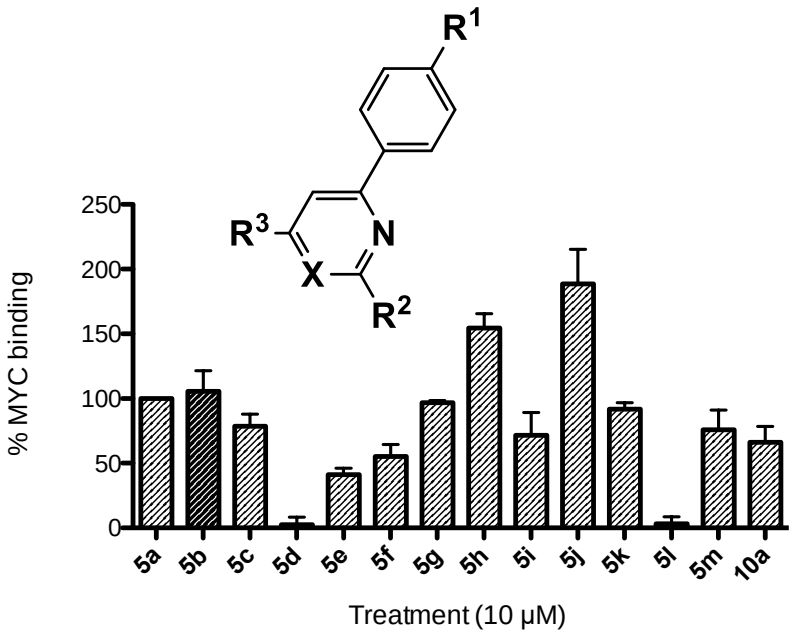

Biophysical screening

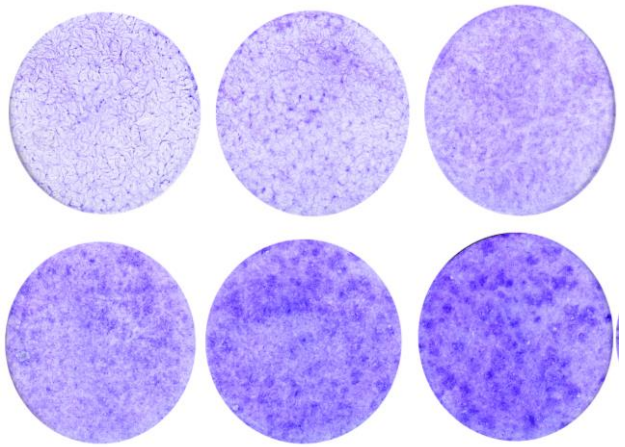

Cellular Efficacy